Visible-light photocatalytic activity and recyclability of N-doped TiO_2 films grown by MOCVD

(Atividade fotocatalítica sob luz visível e reutilização de filmes de TiO_2 dopados com N crescidos por MOCVD)

E. C. de Oliveira[1], R. T. Bento[1]*, O. V. Correa[1], M. F. Pillis[1]
[1]Energy and Nuclear Research Institute, CNEN/SP, University of São Paulo, Av. Prof. Lineu Prestes 2242, S. Paulo, SP Brazil

Abstract

Nitrogen-doped TiO_2 films were grown on borosilicate glass substrates at 400 °C by the metallorganic chemical vapor deposition (MOCVD) for removing dye from water under visible light. The effect of N-doping on the structural, surface, and photocatalytic properties of films was evaluated. X-ray photoelectron spectroscopy (XPS) analyses revealed that 1.56 and 2.44 at% of nitrogen were incorporated into the films by varying the NH_3 flux during the growth. Methyl orange dye degradation experiments showed that the N-doped films presented photoactivity under visible light. The film containing 2.44 at% of nitrogen exhibited the best photocatalytic behavior, with 55% of efficiency. Recyclability tests under visible light showed that the film efficiency dropped gradually after each test. N-TiO_2 films grown by MOCVD have the potential to be used in environmental applications by removing pollutants using a green method under sunlight or even under internal illumination, although its reuse is limited.
Keywords: TiO_2 films, MOCVD, nitrogen-doped TiO_2, photocatalysis, nanostructure, recyclability.

Resumo

O crescimento de filmes de TiO_2 dopados com nitrogênio sobre vidro borossilicato foi efetuado a 400 °C por deposição química de organometálicos em fase vapor (MOCVD) visando a remoção de corantes da água sob luz visível. O efeito da dopagem nas propriedades estruturais, morfológicas e fotocatalíticas dos filmes foi avaliado. Análises por espectroscopia de fotoelétrons excitados por raios X (XPS) revelaram teores de 1,56 e 2,44 at% de nitrogênio nos filmes, ao variar o fluxo de NH_3 durante o crescimento. Experimentos de degradação do corante alaranjado de metila mostraram que os filmes dopados apresentaram fotoatividade em luz visível. O filme contendo 2,44 at% de nitrogênio apresentou o melhor desempenho fotocatalítico, com 55% de eficiência. Os testes de reutilização demonstraram que a eficiência dos filmes diminuiu gradativamente após cada ensaio. Os filmes de N-TiO_2 têm potencial para serem utilizados em aplicações ambientais, removendo poluentes a partir de uma tecnologia verde sob luz solar ou iluminação interna, embora sua reutilização seja limitada.
***Palavras-chave**: filmes de TiO_2, MOCVD, TiO_2 dopado com nitrogênio, fotocatálise, nanoestrutura, reutilização.*

INTRODUCTION

Water is an essential compound for sustaining life and an indispensable resource for human development. Among the different types of contaminants present in water, metals, dyes, and other chemicals coming from the textile industry effluents are widely found. Wastewaters from the textile industry are characterized by being highly colored and toxic. Approximately 50-70% of industrial dye production are azo dyes [1], and about 10-20% is lost during the industrial process and released as effluent [2, 3]. These wastes may generate hazardous by-products resulting from oxidation, hydrolysis, or other chemical reactions [4]. The inappropriate disposal of emerging contaminants, such as pharmaceuticals, antibiotics, and personal care products, besides other industrial waste, has attracted much attention [5-7]. In this way, the development of new technologies for the efficient withdrawal of such compounds from water sources, based on advanced oxidative processes (AOPs), contributes significantly to the treatment and purification of water. AOPs are physicochemical processes characterized by the formation of highly degraded transient species, e.g., $^{\bullet}OH$, H_2O_2, $O_2^{\bullet-}$, ClO_2, O_3, in enough quantities to carry out the chemical transformation of contaminants, and their consequent mineralization [8, 9].

Several studies [10-13] demonstrate the potentiality and possibility of using semiconductor materials and solar radiation on water treatment. Among the various semiconductor materials used in photocatalytic processes, titanium dioxide (TiO_2) has been extensively employed for water treatment by the green method due to its high corrosion resistance, good bactericidal activity, self-cleaning properties, low production cost, and excellent photocatalytic activity [14-16]. According to previous researches

*https://orcid.org/0000-0002-1797-9652

[17], the anatase-TiO_2 phase is the best polymorphic structure for photocatalytic applications due to the higher oxygen adsorption capacity, lower electron (e^-)/hole (h^+) recombination rate, greater surface area, and a higher degree of hydroxylation. Titanium dioxide films can be obtained by several techniques and present different structural properties and morphological characteristics depending on factors such as film thickness, precursor, grain size, growth temperature, and substrate [18]. Metallorganic chemical vapor deposition (MOCVD) is a CVD specific field that uses organometallic compounds as precursors. The structural properties of the films obtained by MOCVD are determined by the deposition parameters and organometallic chemical precursors used [13, 18, 19]. This is an attractive method since it provides good control of stoichiometry and thickness of the films, and uniformity of deposition. Supported TiO_2 films minimize several problems that arise from the practical use of catalyst materials during the photocatalytic process, especially when using a suspension [20]. The catalyst separation from suspensions is a difficult and costly process. In addition, suspended particles tend to aggregate, especially at high concentrations. Nevertheless, film thickness plays an important role in photocatalytic activity. As shown in our previous study [21], TiO_2 films have an ideal thickness in which they perform better in removing dyes from water.

The main advantage of heterogeneous photocatalysis, when compared to conventional water treatment methods, is the possibility of using electromagnetic radiation from the sun to activate the catalyst. The TiO_2 application in heterogeneous photocatalysis is possible due to its semiconductor characteristics and good stability after several catalytic cycles [15, 22]. However, TiO_2 presents high band gap energy (E_g=3.26 eV for anatase-TiO_2), and its photocatalytic activity is observed only under radiation wavelength of λ<380 nm, from the UV radiation, which corresponds to less than 5% of the sunlight [23]. Studies indicate that the doping process narrows the TiO_2 band gap, which allows the activation of the material in the visible light region of the electromagnetic spectrum (400<λ<700 nm), corresponding to 45% of the solar radiation total energy [24]. Teh and Muhammed [23] suggest that the doping of TiO_2 allows a considerable reduction of the electrons (e^-)/hole (h^+) recombination rate, leading to a higher production of hydroxyl radicals (•OH). The narrowing of the TiO_2 band gap region can be obtained by metallic (Ag, Cu, Ni, Fe, Ru) and non-metallic (S, N, C, B, P) species [25, 26], from the formation of intermediate states. Other studies also have shown the possibility of using doped-TiO_2 for the degradation of different dyes, such as reactive triazine dyes (Yellow 84, Red 120, Blue 160) [27], N,N-dimethyl-4-nitrosoaniline (RNO) [28], tartrazine (TRZ), Eriochrome Black-T (EBT) [29], Rhodamine B (RhB) [30], and principally methyl orange dye and methylene blue [31]. Maria Magdalane et al. [32, 33] studied the catalytic properties of the CeO_2/Er_2O_3 and CeO_2/La_2O_3 based binary metal oxide nanostructures on the RhB photodegradation under visible light. It was suggested that the decomposition rate of the dye depends on the pH, irradiation time, and dye concentration. The catalysts presented high photocatalytic activity and stability under UV and visible light. Pan et al. [24] demonstrated that the non-metallic doping of TiO_2 catalyst increases its photocatalytic activity. Among those modified catalysts, nitrogen-doped TiO_2 films presented good results [34, 35]. Shi et al. [36] prepared N-doped TiO_2 by the one-pot hydrothermal method. The photocatalysts exhibited enhanced photoactivity for the methyl orange dye degradation under visible light illumination compared to the undoped TiO_2. Several approaches, such as anodization of a Ti-N alloy [37], anodization in an electrolyte containing N [38], and heat-treatment in ammonia (NH_3) [39] have been employed to introduce N into TiO_2 crystal lattice, and consequently to prepare visible-light-active N-doped TiO_2 photocatalysts.

Some authors [1, 40] suggested that the dye decolorization test by visible-light activated photocatalysts could be influenced by critical problems, such as the dye photosensitization, and the reduction of the available incident light flux to the catalyst [41], due to surface impregnation. Yan et al. [42] showed the inadequacy of dyes as model contaminants for visible light semiconductor photocatalysis, using methylene blue dye and S-doped TiO_2 as a catalyst. Nevertheless, the evaluation of the behavior of N-doped TiO_2 films on the dye decolorization experiments and the study of the possibility of reuse of this photocatalyst on visible light are still important guidelines for searching and practical environmental application for the semiconductor materials. In this study, the effects of the nitrogen doping process on the structural, morphological, and photocatalytic behavior of TiO_2 films grown by MOCVD were investigated. Undoped and nitrogen-doped TiO_2 photocatalytic activity and recyclability experiments were evaluated by monitoring the methyl orange dye degradation under visible light irradiation.

EXPERIMENTAL

Synthesis of the catalysts: TiO_2 films were grown by the MOCVD process in a conventional horizontal homemade reactor described elsewhere [11]. The growth of the films was carried out on borosilicate glass substrates (25x76x1 mm) previously cleaned with 5% H_2SO_4 aqueous solution, rinsed in deionized water, dried in nitrogen (N_2), and immediately inserted into the reactor. Pure TiO_2 and N-doped TiO_2 obtained by MOCVD exhibited different growth rates due to the presence of gaseous ammonia in the atmosphere [43]. The growth time for undoped and N-doped TiO_2 films were 30 and 60 min, respectively, to achieve the film thickness of around 360 nm, an appropriate thickness for photocatalytic application [21]. All films were grown at 400 °C under a pressure of 50 mbar. Previous studies [18, 44] showed that the highest photocatalytic efficiency occurs for the TiO_2 films grown in this condition. Titanium(IV) isopropoxide (TTiP) (Sigma-Aldrich, 99.999%) was used as the titanium and oxygen sources. N_2 was used as both

the carrier gas to transport the TTiP into the system and the purge gas. For the growth of undoped films, the flow rates of TTiP carrier gas and N_2 purge gas were both fixed at 0.5 slm. To obtain the N-doped TiO_2 films, NH_3 was added to the system with flow rates fixed at 0.2 and 0.3 slm, and the N_2 purge gas flux was fixed at 0.8 and 0.7 slm, respectively.

Characterization techniques: the X-ray photoelectron spectroscopy (XPS) was carried out to determine the chemical state of the species at the surface. Thermo Scientific K-Alpha equipment operating with a spot size of 400 μm was used. High-resolution XPS spectra for the principal peaks of Ti 2p, O 1s, and N 1s were collected at pass energy of 50 eV. Chemical deconvolution was done using CasaXPS software [45], and the binding energies were calibrated considering the C 1s reference peak at 284.8 eV, attributed to the adventitious carbon (C-C or C-H) and residual carbon from the metallorganic precursor [44, 46]. X-ray diffraction (XRD) analyses were carried out on a Rigaku Multiflex equipment using CuKα radiation (λ=1.54148 Å), and diffraction angle (2θ) ranging from 10º to 80º, with a step of 0.06º. Surface characteristics of the films were determined by tapping mode-atomic force microscopy (AFM, SPM NanoScope IIIA, Bruker) under ambient conditions. The scan frequency used was 0.9 Hz, and the area was of 5x5 μm. The wettability was evaluated by contact angle measurements (Phoenix-I, SEO) under visible light. The sessile drop method was used by dropping 5 μL of deionized water on the film surface. The experiments were repeated 3 times for each measurement. The cross-section of the films was evaluated by field emission scanning electron microscopy (FE-SEM) in a Jeol JSM-6701F equipment. Fourier-transform infrared (FTIR) spectra of the N-doped films were obtained by a spectrometer (Nexus 870 FT-IR, Thermo Nicolet) in the wavenumber range of 500 to 2500 cm^{-1} at room temperature (25 °C) before and after the photocatalytic cycles of the dye degradation under visible light.

Photocatalytic experiments: the photocatalytic activities of the undoped and N-doped catalysts in the dye degradation were investigated in a homemade reactor described in [44]. Methyl orange (MO) dye was employed as the pollutant model, at the concentration of 0.005 $g.L^{-1}$ and pH=2. Studies [21, 47] suggested that TiO_2 catalysts exhibit better photocatalytic activity under acidic solutions. Four tubular LED lamps (Royal Philips Electron., 4x3 W) were employed as the visible light radiation source. The dye degradation experiments were realized for a total test time of 300 min. The temperature was controlled in the range of 19 to 20 °C during the experiments. The system was kept under bubbling for 1 h in the dark in order to allow the adsorption-desorption equilibrium of the dye molecules on the catalyst surface. A previous study [21] demonstrated that the adsorption-desorption saturation on the TiO_2 film is reached after 40 min. The MO dye concentration changes were examined using a UV-vis spectrophotometer (Global Trade Technol.). Recyclability tests for several photocatalytic cycles were also investigated.

RESULTS AND DISCUSSION

Chemical and structural characterization: the compositional chemical states of TiO_2 and N-doped TiO_2 films grown at 400 °C on borosilicate glass were identified by XPS (Fig. 1). The films contained similar concentrations of Ti, O, and C elements. The results denoted the successful inclusion of N atoms into the TiO_2 films. From the XPS survey (Fig. 1a), the nitrogen content in N-doped TiO_2 films was 1.56 and 2.44 at% for the NH_3 flow rate of 0.2 and 0.3 slm, respectively. Peak fitted XPS N 1s spectra for the 1.56 at% (Fig. 1b) and 2.44 at% (Fig. 1c) of N-doped films revealed 3 major components (Table I). The N state at around 396 eV could be ascribed to Ti-N bonding as the result of the substitution of oxygen ions by nitrogen anions [48, 49]. The peak centered at approximately 397 eV can be attributed to the nitrogen atoms into the N-doped TiO_2 lattice as Ti-O-N structural species [50, 51]. The smaller intensity peak at around 400 eV corresponded to molecularly adsorbed N_2 species on the TiO_2 surface [49, 51]. From the hybrid orbital theory, Liu et al. [52] suggest that the narrowing of the N-doped TiO_2 band gap can be promoted only by the Ti-N bond, from the hybrid orbital formation between the atomic orbitals O 2p and N 2p. Figs. 1d to 1f exhibit the spin-orbit doublet of Ti 2p at around 458 eV (Ti^{4+} $2p_{3/2}$) and 464 eV (Ti^{4+} $2p_{1/2}$), which were associated to anatase-TiO_2 [53]. The small peaks at approximately 457 and 460 eV confirmed the contribution of Ti^{3+} [54]. The high-resolution XPS spectra of O 1s for the undoped and N-doped TiO_2 films showed an asymmetric profile (Figs. 1g to 1i). The Gaussian fitting demonstrated that the surface oxygen was composed of two peaks at: 530.5 eV for undoped film, 529.7 eV for 1.56 at% N-doped film, and 529.8 eV for 2.44 at% N-doped film attributed to oxygen in TiO_2 crystal lattice [44,51]; and at around 531 eV for all films regarded as the adsorbed H_2O [55]. Sun et al. [56] suggested that these shifts of the binding energies observed on the Ti 2p and O 1s regions after the N doping process further confirmed that N atoms might be successfully doped into the TiO_2 lattice.

Fig. 2 shows the XRD patterns of the TiO_2 and N-doped TiO_2 films. The diffraction peaks at (101), (004), (200), (211), (220) and (301) planes corresponded to the anatase-TiO_2 crystalline phase (JCPDS 21-1272) [19, 25, 45]. Undoped TiO_2 presented the [200] preferential growth direction. For the doped films, this characteristic was not observed. Other peaks for the 2.44 at% N-TiO_2 film can be related to the formation of titanium oxynitride phase $TiO_{0.34}N_{0.74}$ (2θ= 32.8°, 40.9°, and 49.1°), according to the JCPDS 44-951 diffraction file [49, 50]. On the 1.56 at% N-TiO_2 XRD pattern, these peaks were not detected, probably due to the little quantity of nitrogen in the film. These results were in accordance with the XPS analyses that revealed anatase-TiO_2 phase for all the films, besides nitrogen incorporation in both doped films.

Cross-sectional analyses: Fig. 3 exhibits the cross-sectional FE-SEM images of undoped and N-doped TiO_2 films. It was observed that the interface between the film

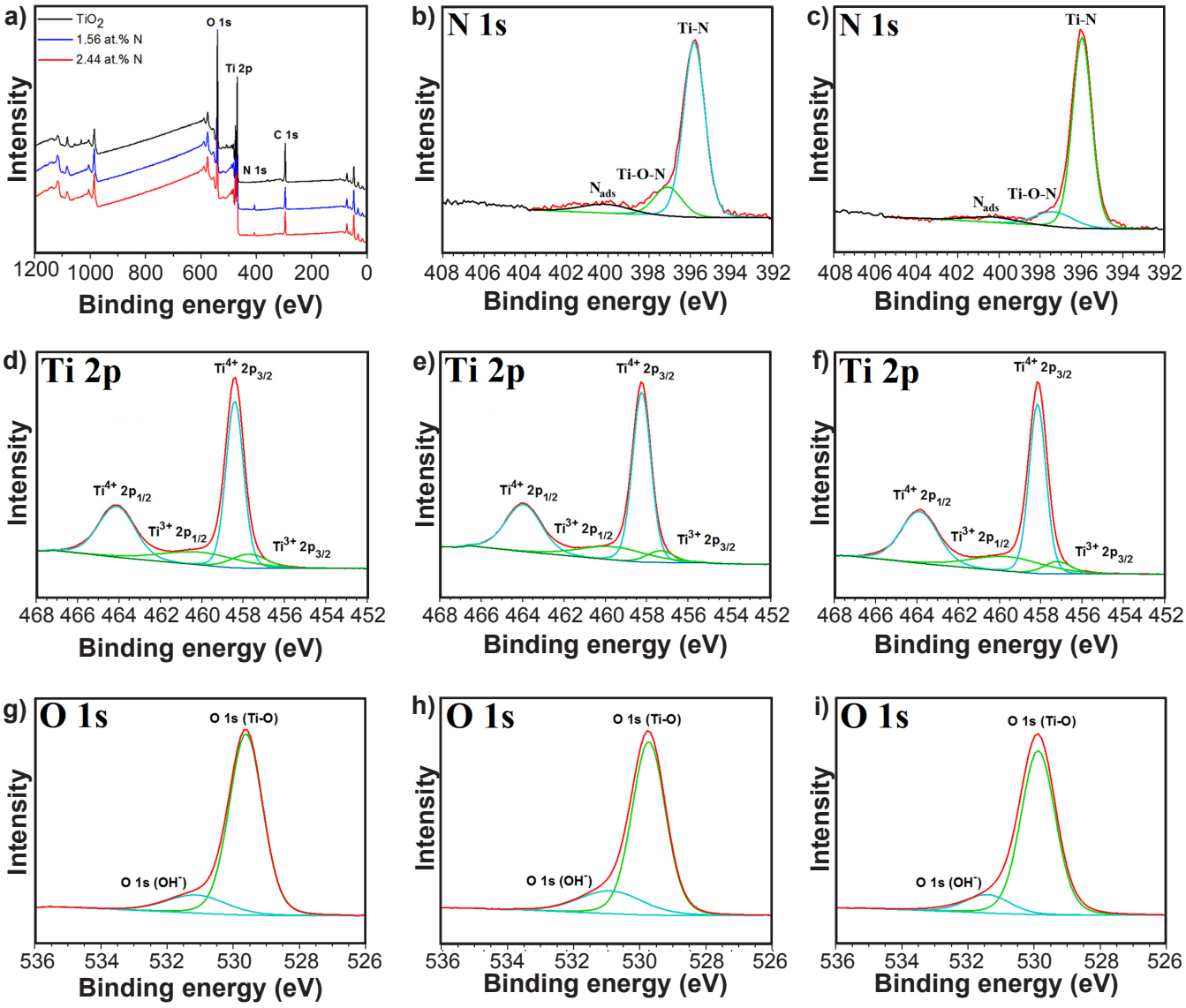

Figure 1: XPS spectra of undoped and N-doped TiO_2 films grown on borosilicate glass substrates at 400 °C by MOCVD: XPS survey spectra (a) and high-resolution XPS spectra of: N 1s region with fitted curves for 1.56 at% N (b), and 2.44 at% N (c) films; Ti 2p region with fitted curves for undoped (d), 1.56 at% N (e), and 2.44 at% N (f) films; and O 1s region with fitted curves for the undoped (g), 1.56 at% N (h), and 2.44 at% N (i) films.

[Figura 1: Espectros de XPS dos filmes de TiO_2 não dopado e dopados com N crescidos em substratos de vidro de borossilicato a 400 °C por MOCVD: espectro exploratório (survey) de XPS (a) e espectros de XPS de alta resolução da: região N 1s com curvas ajustadas para filmes com 1,56 at% de N (b) e 2,44 at% de N (c); região Ti 2p com curvas ajustadas para filmes não dopado (d) e com 1,56 at% de N (e) e 2,44 at% de N (f); e região O 1s com curvas ajustadas para filmes não dopado (g) e com 1,56 at% de N (h) e 2,44 at% de N (i).]

Table I - Binding energies for different chemical species obtained by XPS for undoped and nitrogen-doped TiO_2 films grown by MOCVD.

[Tabela I - Energias de ligação para diferentes espécies químicas obtidas por XPS para filmes de TiO_2 não dopado e dopados com nitrogênio crescidos por MOCVD.]

Film	O 1s		Ti 2p				N 1s		
	Ti-O	Ti-OH	Ti^{4+} $2p_{3/2}$	Ti^{4+} $2p_{1/2}$	Ti^{3+} $2p_{3/2}$	Ti^{3+} $2p_{1/2}$	Ti-N	Ti-O-N	N_{ads}
Undoped TiO_2	530.5	531.3	458.6	464.3	457.9	460.5		-	
1.56 at% N-TiO_2	529.7	531.1	458.4	464.1	457.1	460.8	395.8	397.2	400.3
2.44 at% N-TiO_2	529.8	531.3	458.4	464.1	457.3	460.4	395.9	397.4	400.4

and the substrate was flat and adherent. The films grew perpendicular to the surface of the substrate. The images also revealed the formation of a densified morphology, characteristic of TiO_2 films grown by MOCVD at 400 °C [13, 18, 44]. The undoped TiO_2 film thickness was about 351 nm, while the thickness of the 1.56 and 2.44 at% N-doped TiO_2 films were about 357 and 365 nm, respectively.

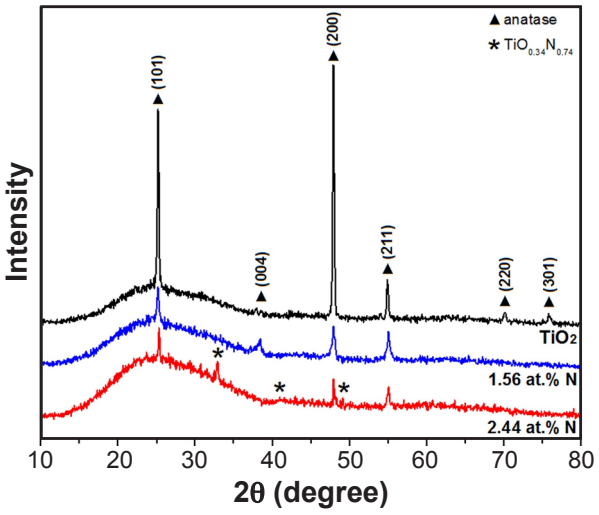

Figure 2: XRD patterns of undoped and N-doped TiO_2 films grown on borosilicate glass substrates at 400 °C by MOCVD.
[Figura 2: Padrões de DRX dos filmes de TiO_2 não dopado e dopados com N crescidos sobre substratos de vidro borossilicato a 400 °C por MOCVD.]

Morphology of the films: both samples of N-doped TiO_2 films obtained at 400 °C for 60 min presented similar morphologies with mean grain size below 100 nm and had some aggregation, as shown in AFM images (Fig. 4). These results suggested the influence of the nitrogen doping process on the morphological characteristics of the films. Compared to the undoped TiO_2, it was observed that the N-doped films exhibited a considerable change in the root-mean-square (RMS) roughness (Table II). Some studies [57, 58] showed a similar trend. This effect promotes a superficial uniformity of the catalyst, which allows increasing its surface area and, consequently, its photocatalytic efficiency [44, 59].

Wettability tests: Fig. 5 shows the images of the contact angle formed between the water drop and the film surfaces. The hydrophilicity of the doped films raised as the nitrogen concentration increased in N-TiO_2 films. The contact angle of water was 62° for the undoped TiO_2 film, and decreased to 53° and 47°, respectively, for 1.56 and 2.44 at% N-doped TiO_2 films. The results suggested that the N doping process can improve the hydrophilicity of TiO_2 films under visible light. Surface wettability is an important property of nanostructured TiO_2 catalysts. Hydrophilic character helps to keep the water molecules closer to the catalyst surface, which facilitates the transfer of electrons [60]. Recently a number of studies reported that the nitrogen-doping process

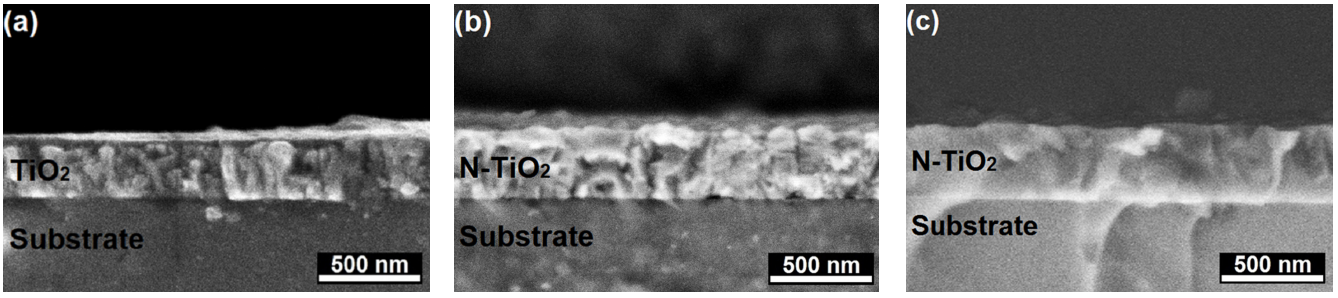

Figure 3: Cross-sectional FE-SEM images of films grown at 400 °C on borosilicate glass substrates by MOCVD for: a) undoped TiO_2 film grown for 30 min; b) 1.6 at% N-doped film, and c) 2.4 at% N-doped film, both grown for 60 min.
[Figura 3: Imagens de MEV-FEG da seção transversal dos filmes crescidos a 400 °C em substrato de vidro borossilicato por MOCVD do: a) filme de TiO_2 não dopado crescido por 30 min; b) filme dopado com 1,56 at% de N, e c) filme dopado com 2,44 at% de N, ambos crescidos por 60 min.]

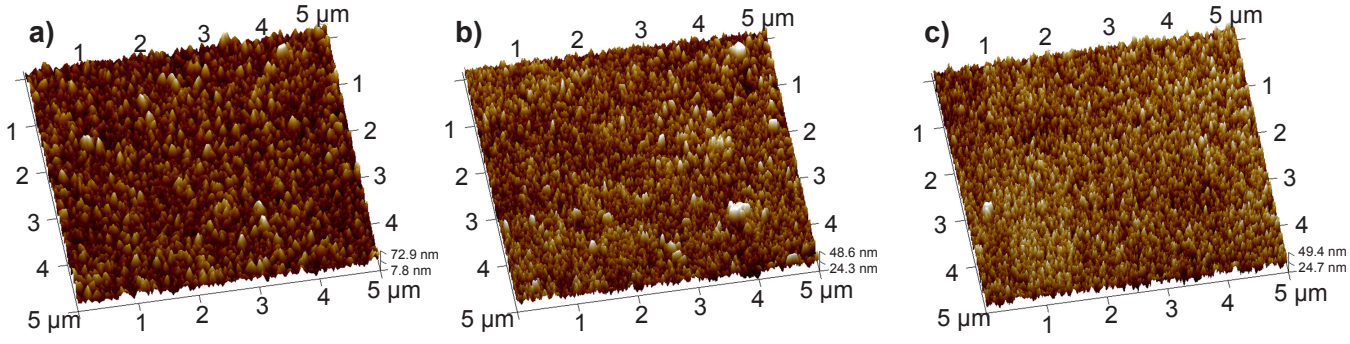

Figure 4: AFM topography images of undoped (a), and 1.56 at% (b), and 2.44 at% (c) N-doped TiO_2 films grown by MOCVD.
[Figura 4: Imagens topográficas de AFM dos filmes de TiO_2 não dopado (a) e dopado com 1,56 at% de N (b) e 2,44 at% de N (c) crescidos por MOCVD.]

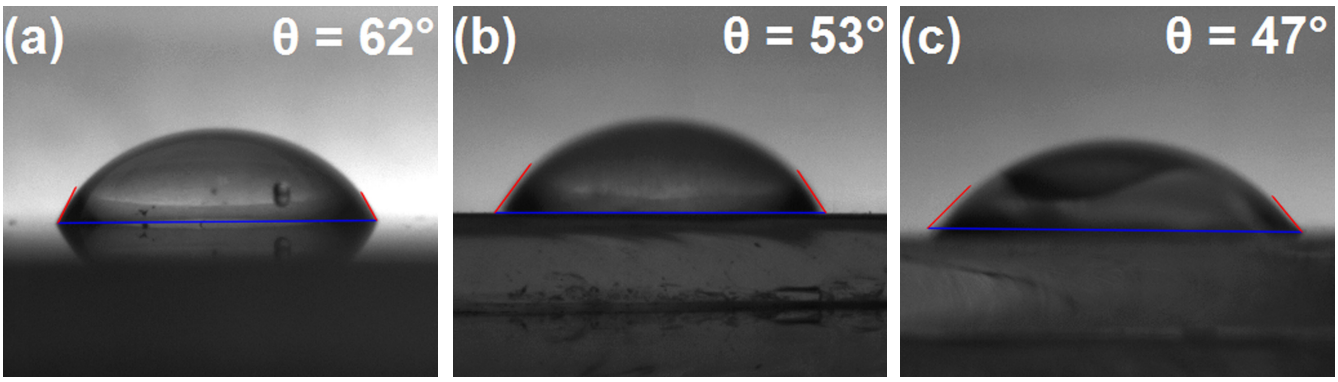

Figure 5: Images of contact angle measurements of undoped (a), and 1.56 at% (b), and 2.44 at% (c) N-doped TiO_2 films grown by MOCVD.
[Figura 5: Imagens de medição de ângulo de contato dos filmes de TiO_2 não dopado (a), e dopados com 1,56 at% de N (b) e 2,44 at% de N (c) crescidos por MOCVD.]

could increase the wettability of TiO_2, which promotes improvement in its surface adsorption of polluting molecules [61-63]. The formation of oxygen vacancies and Ti^{3+} cations on the catalyst surface, as observed in the XPS results, makes the surface more reactive and hydrophilic, and enables the enhanced absorption of visible light [63].

Visible-light-induced degradation of the MO azo dye: the photocatalytic behavior of the undoped and N-doped TiO_2 catalysts on the methyl orange (MO) dye degradation under visible light was evaluated (Fig. 6). The C/C_0 graph exhibited the dye degradation according to the Beer-Lambert relationship [64], where C_0 represents the initial concentration, and C is the dye concentration at each time interval. The photolysis curve demonstrated that without the presence of the catalysts, there was no MO dye degradation. The undoped TiO_2 catalyst did not present photocatalytic activity under visible light. Other studies showed a similar trend [44, 65]. The 2.44 at% N-doped TiO_2 film exhibited the best photocatalytic activity, with a performance of 54.9% of the dye degradation. The 1.56 at% N film degraded 47.2% of dye in the same condition. The results confirmed the influence of the nitrogen concentration on the photocatalytic efficiency of the films under visible light. Sacco et al. [66] evaluated the effect of the methyl orange dye on the N-doped TiO_2 photocatalytic performance. The results showed remarkable efficiencies in the decolorization process, with around 50% of the dye decolorization under visible light, a similar trend found in the present study. Asahi et al. [67] and Ansari et al. [68] suggested that isolated N 2p states are formed above the O 2p valence band from the replacement of oxygen ions by nitrogen anions (E_g=3.06 eV), as well as from the interstitial N-doped TiO_2 (E_g=2.46 eV). After the N-doping process, the energy of visible light (λ>400 nm) became sufficient to excite the electrons from new electronic states to the conduction band, which induced its photocatalytic activity. Some studies [69, 70] related the appearance of a yellowish tone in the N-doped samples, which was also observed in this study. This effect may indicate that the catalyst is absorbing wavelengths in the visible solar spectrum. However, only the absorption of visible light is not sufficient to guarantee a good photodegradation performance of the film. Grain size, roughness, and structural defects also influence its behavior [18]. Table II shows a summary of the N-doping effect on the properties of TiO_2 films. The formation of Ti-O-N revealed from XPS results promoted favorable surface modifications for photocatalytic applications. N-doped TiO_2 films exhibited small grain size, anatase crystalline phase, and higher hydrophilic character than undoped TiO_2, which favored the adsorption of organic molecules on the catalyst surface.

The recyclability capacity of the TiO_2 films is an important requirement for its practical applications on water treatment and purification by using solar radiation. Therefore, the 2.44 at% N-doped TiO_2 film grown by MOCVD at 400 °C was subjected to methyl orange dye degradation under visible light for 300 min at pH=2. Fig. 7 shows the results of 5 photodegradation cycles. After each photocatalytic cycle, the film was rinsed in ethyl alcohol

Table II - Summary of the N doping effect on the morphology c haracteristics and photocatalytic properties of TiO_2 films grown at 400 °C on borosilicate glass substrates by MOCVD.
[Tabela II - Resumo dos efeitos da dopagem com N nas características morfológicas e propriedades fotocatalíticas dos filmes de TiO_2 crescidos a 400 °C em substratos de vidro borossilicato por MOCVD.]

Film	Film thickness (nm)	Mean grain size (nm)	RMS roughness (nm)	Mean contact angle	Visible-light photocatalytic efficiency
Undoped TiO_2	351	123	18.9	62°	Zero
1.56 at% N-TiO_2	357	98	6.7	53°	47.2 %
2.44 at% N-TiO_2	365	83	4.9	47°	54.9 %

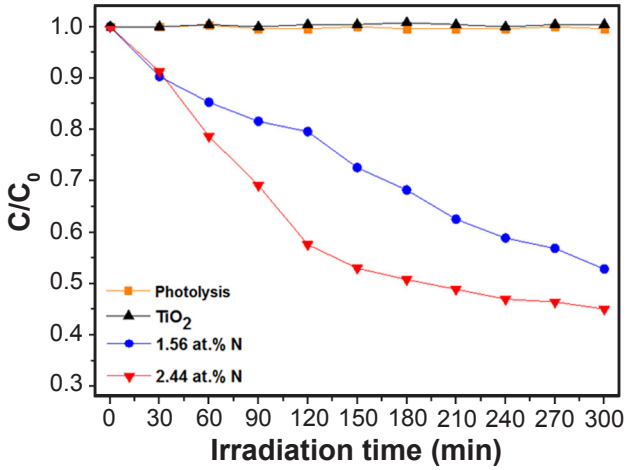

Figure 6: Photocatalysis activity of undoped and nitrogen-doped TiO_2 films grown by MOCVD on the methyl orange dye degradation under visible light irradiation for 300 min.
[Figura 6: Atividade fotocatalítica dos filmes de TiO_2 não dopado e dopados com nitrogênio crescidos por MOCVD na degradação do corante de alaranjada de metila sob irradiação de luz visível por 300 min.]

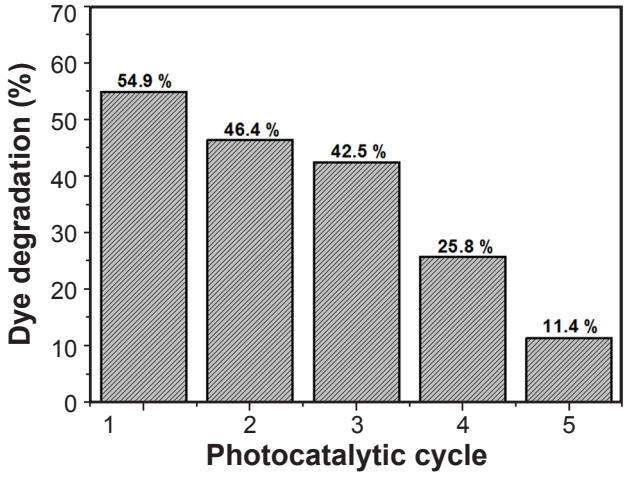

Figure 7: Five recyclability cycles of photocatalytic degradation for methyl orange in the presence of 2.44 at% N-doped TiO_2 film under visible light for 300 min at pH=2. The photocatalytic reactivation of the film surface was performed with ethyl alcohol for 10 min at room temperature and drying in N_2 after each cycle.
[Figura 7: Cinco ciclos de reutilização fotocatalítica de degradação do alaranjado de metila na presença do filme de TiO_2 dopado com 2,44 at% de N em luz visível por 300 min em pH=2. A reativação fotocatalítica da superfície do filme foi realizada com álcool etílico por 10 min em temperatura ambiente e secagem em N_2 após cada ciclo.]

for 10 min at room temperature and then dried in nitrogen. According to a previous study [21], the cleaning and surface reactivation of TiO_2 films with ethyl alcohol is more efficient than the surface cleaning methods using water or acetone. The dye degradation efficiency of the N-doped film dropped to around 43% after the 3rd cycle. In the 4th and 5th cycles, the photocatalytic activity of 25.8% and 11.4%, respectively, were obtained.

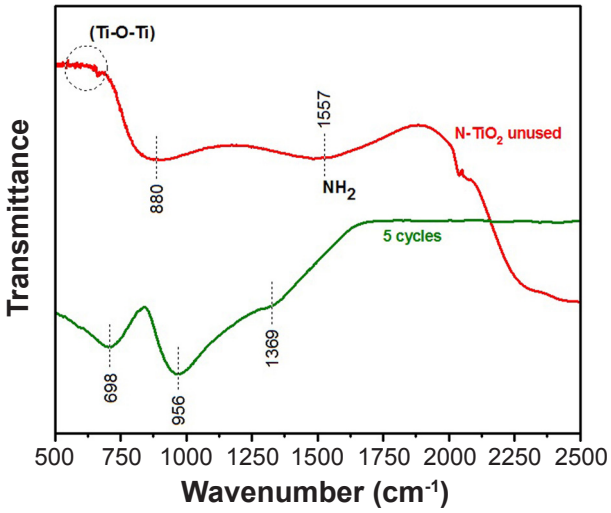

Figure 8: FTIR spectra of N-doped TiO_2 film grown by MOCVD before and after 5 photocatalytic dye degradation cycles under visible light.
[Figura 8: Espectros de FTIR do filme de TiO_2 dopado com N crescido por MOCVD antes e após 5 ciclos de degradação fotocatalítica do corante em luz visível.]

Fig. 8 shows the FTIR spectra of the 2.44 at% N-doped TiO_2 film before and after five photocatalytic cycles of MO dye decolorization. The starting (unused) catalyst exhibited the vibration peaks of Ti-O-Ti symmetrical stretching bond bellow 1000 cm^{-1} [71, 72], and a characteristic absorption band at 1557 cm^{-1}, which can represent the vibration of amino ($-NH_2$) group [73]. However, after the photocatalytic experiments under visible light, there was a change in the FTIR spectrum of the catalyst. The peaks centered at 698 cm^{-1} for C-S stretching vibration of the benzene ring, 956 cm^{-1} for aromatic C-H vibration, and 1369 cm^{-1} for C-N vibration confirmed the aromatic and azo nature of the dye [74, 75]. The results suggested the dye molecule impregnation on the catalyst surface after its use. The impregnated dye shielded the N-doped TiO_2 surface from visible light irradiation [41] and limited its reuse.

CONCLUSIONS

The structural, morphological, and photocatalytic characteristics of undoped and nitrogen-doped TiO_2 films grown at 400 °C on borosilicate glass substrates by the metallorganic chemical vapor deposition (MOCVD) process were evaluated. The nitrogen-doping promoted modifications on the surface of the films. The photocatalytic experiments demonstrated that the N-doped TiO_2 films can degrade methyl orange dye under visible light. This behavior corroborated the influence of the film morphological characteristics on the photocatalytic efficiency. Undoped TiO_2 film did not show photoactivity under visible light. The results revealed that the 2.44 at% N-doped TiO_2 film exhibited the best photocatalytic activity under visible light, with 54.9% of dye degradation, 16 % more efficient than the 1.56 at% N-doped film. Recyclability tests indicated a

reduction of film efficiency for dye degradation after each cycle. Fourier-transform infrared (FTIR) spectroscopy showed that the catalyst surface was impregnated by the dye, which limited the reuse of the N-doped TiO_2 film.

ACKNOWLEDGMENTS

The authors are grateful to the Brazilian agencies CNPq (Proc. 168935/2018-0) and FAPESP (Proc. 05/55861-4) for financial support. This research used resources of the Brazilian Nanotechnology National Laboratory (LNNano). The Nanostructured Materials Laboratory staff is acknowledged for kindly make available the XPS equipment and for the assistance during the experiments.

REFERENCES

[1] N. Shaham-Waldmann, Y. Paz, Mater. Sci. Semicond. Process. **42** (2016) 72.
[2] N. Delegan, R. Pandiyan, S. Komtchou, A. Dirany, P. Drogui, M.A. El Khakani, J. App. Phys. **123** (2018) 205101.
[3] I.M.C. Gonçalves, A. Gomes, R. Brás, M.I.A. Ferra, M.T.P. Amorim, R.S. Porter, Color. Technol. **116** (2000) 393.
[4] Y.K. Abdel-Maksoud, E. Imam, A.R. Ramadan, Catal. Today **313** (2018) 55.
[5] S. Khaoulani, H. Chaker, C. Cadet, E. Bychkov, L. Cherif, A. Bengueddach, S. Fourmentin, C. R. Chim. **18** (2015) 23.
[6] N. Delegan, R. Pandiyan, S. Komtchou, A. Dirany, P. Drogui, J. Appl. Phys. **123** (2018) 1.
[7] Y.K. Abdel-Maksoud, E. Imam, A.R. Ramadan, Catal. Today **313** (2018) 55.
[8] K.M. Reza, A.S.W. Kurny, F. Gulshan, Appl. Water Sci. **7** (2017) 1569.
[9] R. Guz, C. Moura, M.A.A. Cunha, Environ. Sci. Pollut. Res. Int. **24** (2017) 6055.
[10] O. Sacco, V. Vaiano, L. Rizzo, D. Sannino, J. Clean. Prod. **175** (2018) 38.
[11] R.T. Bento, M.F. Pillis, in "Titanium dioxide: material for a sustainable environment", D. Yang (Ed.), InTech, London (2018) 211.
[12] B. Appavu, S. Thiripuranthagan, S. Ranganathan, E. Erusappan, K. Kannan, Ecotoxicol. Environ. Saf. **151** (2018) 118.
[13] A.J. Gardecka, C. Bishop, D. Lee, S. Corby, I.P. Parkin, A. Kafizas, S. Krumdieck, Appl. Catal. B **224** (2018) 904.
[14] Y. Cao, Z. Fu, W. Wei, L. Zou, T. Mi, D. He, C. Yan, X. Liu, Y. Zhu, L. Chen, Y. Sun, Appl. Surf. Sci. **355** (2015) 1289.
[15] S. Athalathil, B. Erjavec, R. Kaplan, F. Stuber, C. Bengoa, J. Font, A. Fortuny, A. Pintar, A. Fabregat, J. Hazard. Mater. **300** (2015) 406.
[16] N. Kumar, S.N. Hazarika, S. Limbu, R. Boruah, P. Deb, N.D. Namsa, S.K. Das, Micropor. Mesopor. Mater. **213** (2015) 181.
[17] K. Tanaka, M.F. Capule, T. Hisanaga, Chem. Phys. Lett. **187** (1991) 73.
[18] R.T. Bento, A. Ferrus Filho, M.F. Pillis, Rev. Bras. Inov. Tecnol. Saúde **7** (2017) 4.
[19] H.O. Pierson, *Handbook of chemical vapor deposition (CVD): principles, technology and applications*, 2nd ed., Noyes Publ. (1999).
[20] X. Zhang, M. Zhou, L. Lei, Mater. Chem. Phys. **91** (2005) 73.
[21] B.A. Marcello, O.V. Correa, R.T. Bento, M.F. Pillis, J. Braz. Chem. Soc. **31** (2020) 1270.
[22] J. Ângelo, P. Magalhães, L. Andrade, A. Mendes, Appl. Surf. Sci. **387** (2016) 183.
[23] C.M. Teh, A.R. Mohamed, J. Alloys Compd. **509**, 5 (2011) 1648.
[24] L. Pan, J.-J. Zou, S. Wang, Z.-F. Huang, X. Zhang, L. Wang, Appl. Surf. Sci. **268** (2013) 252.
[25] M. Dhayal, R. Kapoor, P.G. Sistla, R.R. Pandey, S. Kar, K.K. Saini, G. Pande, Mater. Sci. Eng. C **37** (2014) 99.
[26] J. Zhang, G.-F. Huang, D. Li, B.-X. Zhou, S. Chang, A. Pan, W.-Q. Huang, Appl. Phys. A **122**, 12 (2016) 1.
[27] A. Selvaraj, S. Sivakumar, A.K. Ramasamy, V. Balasubramanian, Res. Chem. Intermediat. **39** (2013) 2287.
[28] A. Pipi, G. Byzynski, L. Ruotolo, Mat. Res. **20** (2017) 628.
[29] V. Vaiano, O. Sacco, G. Iervolino, D. Sannino, P. Ciambelli, R. Liguori, A. Rubino, Appl. Catal. B **176-177** (2015) 594.
[30] K. Kasinathan, J. Kennedy, M. Elayaperumal, M. Malik, Sci. Rep. **6** (2016) 38064.
[31] L. Mei, R. Zuo, J. Xie, L. Liao, H. Ding, Adv. Mater. Sci. Eng. **2014** (2014) 1.
[32] C. Maria Magdalane, K. Kaviyarasu, A. Raja, M.V. Arularasu, G.T. Mola, A.B. Isaev, M. Maaza, J. Photochem. Photobiol. B Biol. **185** (2018) 275.
[33] C. Maria Magdalane, K. Kaviyarasu, N. Matinise, N. Mayedwa, N. Mongwaketsi, D. Letsholathebe, B. Jeyaraj, S. Afr. J. Chem. Eng. **26** (2018) 49.
[34] F. Maury, F.-D. Duminica, Surf. Coat. Technol. **205**, 5 (2010) 1287.
[35] T.C. Jagadale, S.P. Takale, R.S. Sonawane, H.M. Joshi, S.I. Patil, B.B. Kale, S.B. Ogale, J. Phys. Chem. C **112** (2008) 14595.
[36] J.W. Shi, H.Y. Ai, J.W. Chen, H.J. Cui, S. Yang, S. Li, M.L. Fu, J. Mol. Catal. A Chem. **395** (2014) 420.
[37] D. Kim, S. Fujimoto, P. Schmuki, H. Tsuchiya, Electrochem. Commun. **10** (2008) 910.
[38] Y. Su, X. Zhang, M. Zhou, S. Han, L. Lei, J. Photochem. Photobiol. A **194** (2008) 152.
[39] A. Petala, D. Tsikritzis, M. Kollia, S. Ladas, S. Kennou, D.I. Kondarides, Appl. Surf. Sci. **305** (2014) 281.
[40] M. Rochkind, S. Pasternak, Y. Paz, Molecules **20** (2014) 88.
[41] S. Bae, S. Kim, S. Lee, W. Choi, Catal. Today **224** (2014) 21.
[42] X. Yan, T. Ohno, K. Nishijima, R. Abe, B. Ohtani, Chem. Phys. Lett. **429** (2006) 606.
[43] E.A. Souza Filho, E.F. Pieretti, R.T. Bento, M.F. Pillis, J. Mater. Res. Technol. **9** (2020) 922.

[44] R.T. Bento, O.V. Correa, M.F. Pillis, J. Eur. Ceram. Soc. **39**, 12 (2019) 3498.
[45] J. Walton, P. Wincott, N. Fairley, A. Carrick, *Peak fitting with CasaXPS: a Casa pocket book*, Accolyte Sci., Knutsford (2010).
[46] D. Duc La, A. Rananaware, H.P. NguyenThi, L. Jones, S.V. Bhosale, Adv. Nat. Sci. Nanosci. Nanotechnol. **8** (2017) 15009.
[47] A. Ahmadpour, M. Zare, M. Behjoomanesh, M. Avazpour, Adv. Environ. Technol. **3** (2015) 121.
[48] J. Ananpattarachai, P. Kajitvichyanukul, S. Seraphin, J. Hazard. Mater. **168** (2009) 253.
[49] M.A. Baker, H. Fakhouri, R. Grilli, J. Pulpytel, W. Smith, F. Arefi-Khonsari, Thin Solid Films **552** (2014) 10.
[50] N.C. Saha, H.G. Tompkins, J. Appl. Phys. **72** (1992) 3072.
[51] J. Du, G. Zhao, Y. Shi, Haoyang, Y. Li, G. Zhu, Y. Mao, R. Sa, W. Wang, Appl. Surf. Sci. **273** (2013) 278.
[52] J. Liu, S. Zhao, H. Wang, Y. Cui, S. Liu, W. Jiang, N. Wang, C. Liu, W. Chai, W. Ding, Mater. Lett. **197** (2017) 28.
[53] F.D. Duminica, F. Maury, R. Hausbrand, Surf. Coat. Technol. **201** (2007) 9349.
[54] M. Li, Z. Xing, J. Jiang, Z. Li, J. Kuang, J. Yin, N. Wan, Q. Zhu, W. Zhou, Mater. Chem. Phys. **219** (2018) 303.
[55] S.M. El-Sheikh, T.M. Khedra, A. Hakkib, A.A. Ismaila, W.A. Badawy, D.W. Bahnemann, Sep. Purif. Technol. **173** (2017) 258.
[56] L. Sun, J. Cai, Q. Wu, P. Huang, Y. Su, C. Lin, Electrochim. Acta **108** (2013) 525.
[57] M. Chekini, M.R. Mohammadizadeh, S.M. Vaez Allaei, Appl. Surf. Sci. **257** (2011) 7179.
[58] M.-C. Wang, H.-J. Lin, C.-H. Wang, H.-C. Wu, Ceram. Int. **38**, 1 (2012) 195.
[59] I. Oja Acik, V. Kiisk, M. Krunks, I. Sildos, A. Junolainen, M. Danilson, A. Mere, V. Mikli, Appl. Surf. Sci. **261** (2012) 735.
[60] K.G. Grigorov, I.C. Oliveira, H.S. Maciel, M. Massi, M.S. Oliveira Jr., J. Amorim, C.A. Cunha, Surf. Sci. **605** (2011) 775.
[61] L.G. Devi, R. Kavitha, Appl. Catal. B **140** (2013) 559.
[62] J. Wang, B. Mao, J.L. Gole, C. Burda, Nanoscale **2** (2010) 2257.
[63] W. Yu, X. Liu, L. Pana, J. Li, J. Liu, J. Zhang, P. Li, C. Chen, Z. Sun, Appl. Surf. Sci. **319** (2014) 107.
[64] V. Belessi, G. Romanos, N. Boukos, D. Lambropoulou, C. Trapalis, J. Hazard. Mater. **170** (2009) 836.
[65] H. Shen, L. Mi, P. Xu, W. Shen, P.-N. Wang, Appl. Surf. Sci. **253** (2007) 7024.
[66] O. Sacco, M. Stoller, V. Vaiano, P. Ciambelli, A. Chianese, D. Sannino, Int. J. Photoenergy **2012** (2012) 1.
[67] R. Asahi, T. Morikawa, T. Ohwaki, K. Aoki, Y. Taga, Science **294** (2001) 269.
[68] S.A. Ansari, M.M. Khan, M.O. Ansari, M.H. Cho, New J. Chem. **40**, 4 (2016) 3000.
[69] J. Geng, D. Yang, J. Zhu, D. Chen, Z. Jiang, Mater. Res. Bull. **44** (2009) 146.
[70] Y.-P. Peng, S.-L. Lo, H.-H. Ou, S.-W. Lai, J. Hazard. Mater. **183** (2010) 754.
[71] S. Amreetha, S. Dhanuskodi, A. Nithya, K. Jothivenkatachalam, RSC Adv. **6** (2016) 7854.
[72] B. Tian, Y. Qian, B. Hu, J. Sun, Z. Du, J. Mater. Res. **27** (2012) 2408.
[73] H. Li, H. Liu, A. Fu, G. Wu, M. Xu, G. Pang, X. Zhao, Materials **9** (2016) 849.
[74] D.C. Kalyani, A.A. Telke, S.P. Govindwar, J.P. Jadhav, Water Environ. Res. **81** (2009) 298.
[75] T. Shen, C. Jiang, C. Wang, J. Sun, X. Wang, X. Li, RSC Adv. **5** (2015) 58704.
(Rec. 10/03/2020, Rev. 15/05/2020, Ac. 07/06/2020)